Airborne Wind Energy Based on Dual Airfoils

Mario Zanon, Sébastien Gros, Joel Andersson, and Moritz Diehl

***Abstract*— The airborne wind energy (AWE) paradigm proposes to generate energy by flying a tethered airfoil across the wind flow at a high velocity. Although AWE enables flight in higher altitude and stronger wind layers, the extra drag generated by the tether motion imposes a significant limit to the overall system efficiency. To address this issue, two airfoils with a shared tether can reduce overall system drag. Although this technique may improve the efficiency of AWE systems, such improvement can only be achieved through properly balancing the system trajectories and parameters. This brief tackles that problem using optimal control. A generic procedure for modeling multiple-airfoil systems with equations of minimal complexity is proposed. A parametric study shows that at small and medium scales, dual-airfoil systems are significantly more efficient than single-airfoil systems, but they are less advantageous at very large scales.**

***Index Terms*— Airborne wind energy (AWE), dual airfoil, large-scale optimization, power optimization.**

I. Introduction

TO OVERCOME the major difficulties posed by the growing size and mass of conventional wind turbine generators [5], [16], the airborne wind energy (AWE) paradigm proposes to eliminate the structural elements that are not directly involved in power generation. An emerging consensus recognizes crosswind flight as the most efficient approach to AWE [17]. Crosswind flight extracts power from the airflow by flying an airfoil tethered to the ground at a high velocity across the wind direction. Power can be generated by: 1) performing a cyclical variation of the tether length, together with cyclical variation of the tether tension or 2) using onboard turbines, transmitting the power to the ground via the tether. In this brief, option 2) is considered, as investigated by Makani Power [18].

Because it involves a much lighter structure, a major advantage of power generation based on crosswind flight over conventional wind turbines is that higher altitude can be reached and a larger swept area can be achieved, thereby reaching wind resources that cannot be tapped by conventional wind turbines [11].

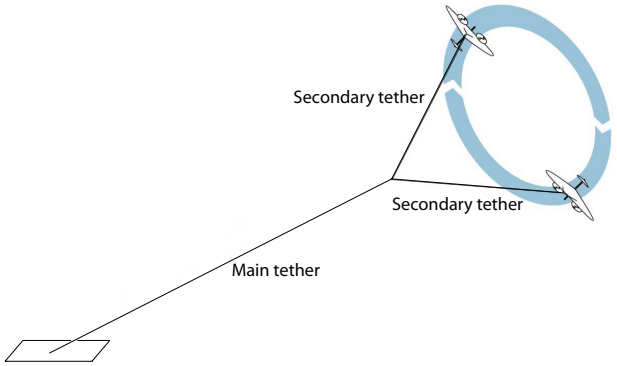

Fig. 1. Schematic diagram of a dual-airfoil AWE system (see. [21], Fig. 3).

Unfortunately, the drag because of the motion of the tether during crosswind flight has a significant impact on the system performance. To tackle this issue, the dual-airfoil design was first introduced in [21] and later investigated in [15], [22], and [25]. The key idea of the dual-airfoil design is to fly two airfoils connected on a single main tether (Fig. 1) in a balanced manner. Therefore, only the shorter secondary tethers move at a high velocity and generate drag, whereas the motion of the main tether is negligible.

Although the dual-airfoil design has the potential to reduce the problem of tether drag for AWE systems, the system design and trajectory must be carefully selected so as to fully exploit the gains of reducing the tether drag. More precisely: 1) the airfoil trajectories must balance the forces on the main tether so as to minimize its motion, maintain the optimal airfoil velocities, and maintain an optimal angle between the secondary tethers; 2) the aerodynamic forces yielded by onboard power generation must be appropriately chosen so as to maximize the system efficiency; 3) the tether lengths must be chosen so as to achieve the best trade-off between reaching higher altitude and adding airborne mass; and 4) the tether diameters must be selected so as to achieve the best trade-off between reducing the drag and withstanding the forces in the system.

Defining the optimal system parameters and trajectory is a highly involved problem that is best cast in the framework of optimal control. Single- and multiple-kite models were proposed in [7], [12]–[15], and [24]. This brief, however, proposes a generic modeling procedure for multiple-airfoil AWE systems, including a finite element model (FEM) for the tethers that is well-suited for optimal control and that produces

Manuscript received January 15, 2012; revised March 2, 2013; accepted March 26, 2013. Manuscript received in final form April 4, 2013. Date of publication May 7, 2013; date of current version June 14, 2013. This work was supported in part by the Research Council KUL under PFV/10/002 Optimization in Engineering Center OPTEC, GOA/10/09 MaNet and GOA/10/11 Global real-time optimal control of autonomous robots and mechatronic systems; the Flemish government under IOF/KP/SCORES4CHEM; FWO Ph.D./Post-Doctoral grants and projects G.0320.08 (convex MPC) and G.0377.09 (Mechatronics MPC); IWT Ph.D. grants and projects SBO LeCoPro; the Belgian Federal Science Policy Office under IUAP P7 (DYSCO, Dynamical systems, control and optimization, 2012-2017); the EU under FP7-EMBOCON (ICT-248940), FP7-SADCO (MC ITN-264735), ERC ST HIGHWIND (259 166), Eurostars SMART, and ACCM. Recommended by Associate Editor L. Fagiano.

The authors are with the Electrical Engineering Department and the Optimization in Engineering Center, K. U. Leuven, Leuven-Heverlee B-3001, Belgium (e-mail:: mario.zanon@esat.kuleuven.be; sgros@esat.kuleuven.be; joel.andersson@esat.kuleuven.be; moritz.diehl@esat.kuleuven.be).

Color versions of one or more of the figures in this paper are available online at http://ieeexplore.ieee.org.

Digital Object Identifier 10.1109/TCST.2013.2257781

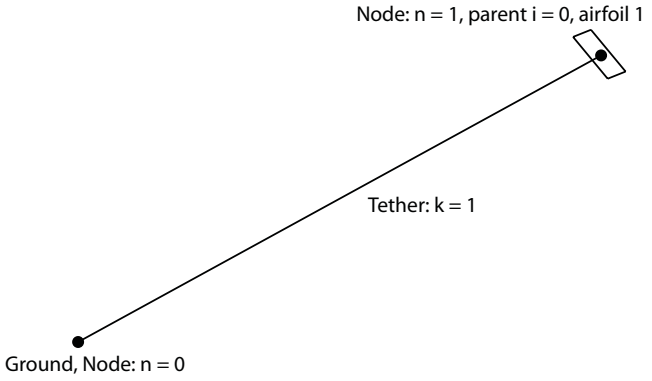

Fig. 2. Schematic diagram of the single-airfoil architecture with $N = 1$, $\mathcal{A} = \{1\}$, and $\mathcal{F}(1) = 0$.

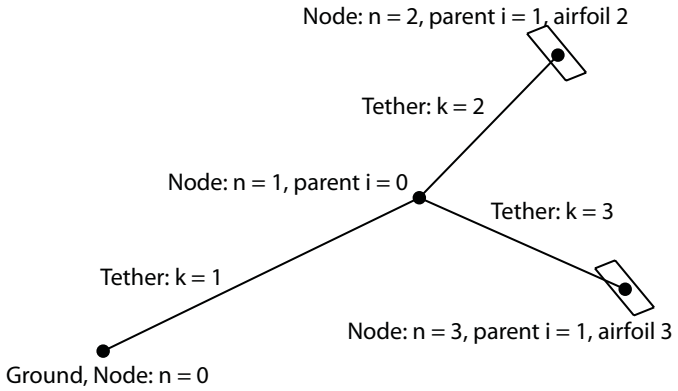

Fig. 3. Schematic diagram of the dual-airfoil architecture with $N = 3$, $\mathcal{A} = \{2, 3\}$, $\mathcal{F}(1) = 0$, $\mathcal{F}(2) = 1$, and $\mathcal{F}(3) = 1$.

model equations of minimal complexity, so as to reduce the computational burden of evaluating the model sensitivities. The resulting model has 41 states for the single airfoil and 207 states for the dual airfoils. A parametric study of the performance of a dual-airfoil system versus a single-airfoil system is presented.

This brief is organized as follows. Initially a generic modeling procedure for multiple-airfoil systems is proposed and discussed in Section II. Section III describes the power-generation optimization problem, the solution approach used to compute power-generating trajectories, and the software used to perform the optimization. Section IV describes a comparison between optimal power generation based on single and dual airfoils for different system scales. Finally, Section V summarizes a conclusion and outlines further developments.

A. Contributions of This Brief

A generic modeling procedure of minimal computational complexity for multiple-airfoil systems is developed. A large-scale model of single and dual airfoils is developed, including a FEM of the tethers. An optimization procedure to determine the optimal trajectories and design parameters is proposed. A comparison of a dual-airfoil versus a single-airfoil AWE system is presented.

II. System Model

The airfoils are inertially modeled as point-masses. An orthonormal right-handed reference frame $e = \{e_x, e_y, e_z\}$ attached to the ground is chosen to generate the Cartesian coordinate system defining the positions of the airfoils. The frame e is chosen such that 1) the wind is blowing in the e_x-direction and 2) the vector e_z is opposed to the gravitational acceleration vector g. The origin of the coordinate system coincides with the attachment point of the main tether to the ground. In the following, a general procedure for the modeling of multiple-airfoil systems is proposed. Both single and dual airfoils are special cases of this formulation, as shown in Figs. 2 and 3.

A. System Architecture

The system is described as a set of N nodes $n \in \{0, \ldots, N\}$ with associated coordinate vectors $X_n \in \mathbb{R}^3$. The fixed node $X_0 = [0,\ 0,\ 0]^T$ is the attachment point of the AWE system to the ground. The subset $\mathcal{A} \subset \{1, \ldots, N\}$ of the set of nodes describes the nodes associated to the airfoils. Assuming a tree structure, to each node $n \in \{1, \ldots, N\}$ a single tether $k = n$ is associated, and the parent node i to which the tether is attached is defined by the map $i = \mathcal{F}(n)$. See Figs. 2 and 3 for an illustration. The system architecture is then defined by the number of nodes N, the set $\mathcal{A}$, and the map $\mathcal{F}$. The proposed formulation allows for treelike system architectures only.

In the following, the component-wise notation $X_n = [x_n,\ y_n,\ z_n]^T$ of the node coordinate vectors X_n is used. The position of the node n is given by $\mathcal{P}_n = x_n e_x + y_n e_y + z_n e_z$. Each tether $k = 1, \ldots, N$ has associated length l_k and diameter d_k.

B. Airfoil Model

For any node $n \in \{0, \ldots, N\}$, we define the velocity relative to the airmass as follows:

$$v_n = (\dot{x}_n - W)\, e_x + \dot{y}_n\, e_y + \dot{z}_n\, e_z$$

where $W \in \mathbb{R}$ is the local wind velocity in the e_x direction. A generalization of this formulation to a 3-D wind field is straightforward. If $n \in \mathcal{A}$, the norms of the lift and drag forces acting on the airfoil n are given by [20]

$$\|F_L^n\| = \frac{1}{2}\rho S C_L^n \|v_n\|^2, \quad \|F_D^n\| = \frac{1}{2}\rho S C_D^n \|v_n\|^2$$

where C_L^n and C_D^n are the lift and drag coefficients of the airfoil, ρ is the air density, and S is the airfoil surface.

The lift force is defined to be orthogonal to the relative velocities v_n of the airfoil. In addition, it is assumed in this model that the lift force is orthogonal to the airfoil transversal axis [8], [20]. Airfoil n is linked to its parent node $i = \mathcal{F}(n)$ by tether n. One can form the unitary coordinate vector as follows:

$$e_r^n = \frac{X_n - X_i}{\|X_n - X_i\|}, \quad i = \mathcal{F}(n)$$

and introduce the following definition of the transversal and lift axis as follows:

$$e_T^n = \frac{v_n \times e_r^n}{\|v_n \times e_r^n\|} \qquad f_L^n = e_T^n \times v_n.$$

It can be observed that vector e_T^n is normed to 1, thus vector f_L^n is normed to $\|v_n\|$. Because f_L^n is orthogonal to the relative velocity v_n and lies in the plane spanned by $\{e_r^n, v_n\}$, if the airfoil is not tilted with respect to vector e_r^n, the lift force acts along vector f_L^n. Introducing the roll angle ψ_i describing the tilting of the lift force around the axis v_n, the lift force can be defined by

$$F_L^n = \frac{1}{2}\rho S C_L^n \left(\cos(\psi_i) f_L^n \|v_n\| - \sin(\psi_i) e_T^n \|v_n\|^2\right).$$

By definition F_{L}^n is always orthogonal to v_n, and lies in the plane defined by $\{e_r^n, v_n\}$ if $\psi_i = 0$.

The airfoil drag force is opposed to the relative velocity, and is readily given by

$$F_D^n = -\frac{1}{2}\rho S C_D^n \|v_n\| v_n.$$

The drag generated by the onboard turbines can be modeled as follows:

$$F_G^n = -\kappa_n \|v_n\| v_n$$

where $\dot{\kappa}_n(t) = u_{\kappa_n(t)}$, $u_{\kappa_n(t)}$ is a control variable and we assume the generated force is opposed to the relative velocity. The resulting aerodynamic power is as follows:

$$P_n = v_n^T F_G^n = -\kappa_n \|v_n\|^3.$$

The resulting airfoil aerodynamic force acting on airfoil n is given by $F_A^n = F_L^n + F_D^n + F_G^n$.

In this model, it is assumed that the time-derivative of the lift coefficient is directly controlled, and the drag coefficient C_{D}^n is approximated by [8], [20]

$$C_D^n = C_D^0 + C_D^I \left(C_L^n\right)^2$$

where C_D^0 and C_D^I are the airfoil drag and induced-drag coefficients, respectively.

The kinetic and potential energy functions associated with the airfoil dynamics are as follows:

$$\mathcal{T}_A^n = \frac{1}{2} M_A \|\dot{X}_n\|^2, \quad \mathcal{V}_A^n = M_A g z_n$$

where M_A is the airfoil mass, and the Lagrange function for the airfoils reads as follows:

$$\mathcal{L}_A = \mathcal{T}_A - \mathcal{V}_{\mathrm{A}}, \quad \mathcal{T}_A = \sum_{n\in A} \mathcal{T}_A^n, \quad \mathcal{V}_A = \sum_{n\in A} \mathcal{V}_A^n.$$

C. Wind and Atmosphere Model

Assuming a laminar wind flow with a logarithmic wind shear model blowing uniformly in the e_x-direction, the free-flow windspeed W_∞ at altitude z is given by [19]

$$W_\infty(z) = W_0 \frac{\log(z/z_r)}{\log(z_0/z_r)} \tag{1}$$

where $W_0 \in \mathbb{R}$ is the wind velocity at altitude z_0 and z_r is the ground roughness.

Consider the drop of density with altitude the following atmospheric model is introduced [2] as follows:

$$T(z) = T_0 - T_L z$$
$$P(z) = P_0 \left(1 - \frac{T_L z}{T_0}\right)^{\frac{gM_a}{RT_L}}$$
$$\rho(z) = \frac{P M_a}{RT}$$

where T_0 is the sea level standard temperature, T_L is the temperature lapse rate, P_0 is the pressure at sea level, M_a is the molar air density, and R is the universal gas constant.

D. Tether Model

In the proposed formulation, the tethers are modeled with a lumped-mass FEM. For a rigid tether $k \in \{1, \ldots, N\}$ of length l_k, density ρ_c, diameter d_k, we define N_k elements linked by massless rigid links, where link k, j connects elements k, j and $k, j+1$. Based on this notation, the position of the endpoint X_{k,N_k} of each tether k coincides with the position X_k of node k. The index j ranges from 1 to N_k when it refers to the elements and from 1 to $N_k - 1$ when it refers to the links between elements. In the proposed model, all links have the same length $l_{k,j} = l_k/(N_k - 1)$ and each element k, j with $2 < j < N_k$ has mass $m_{k,j} = m_k/(N_k - 1)$, whereas $m_{k,1} = m_{k,N_k} = m_k/(2(N_k - 1))$. The tether kinetic and potential energy functions are read as follows:

$$\mathcal{T}_T^k = \sum_{j=1}^{N_k} \frac{1}{2} m_{k,j} \|\dot{X}_{k,j}\|^2$$
$$\mathcal{V}_T^k = \sum_{j=1}^{N_k} m_{k,j} g z_{k,j}$$

where $m_{k,j}$ is the mass associated with each element and $\dot{X}_{k,j}$ and $z_{k,j}$ are, respectively, its velocity and height.

The tether drag on each tether section k, j is given by

$$F_S^{k,j} = -\frac{1}{2}\rho_{k,j} d_k l_{k,j} C_{\mathrm{T}} \|v_{k,j}\| v_{k,j}$$

where C_T is the drag coefficient of a cylinder, $l_{k,j}$ is the length of link k, j, and $v_{k,j}$ is the velocity of its midpoint, computed as follows:

$$v_{k,j} = \frac{\dot{X}_{k,j} + \dot{X}_{k,j+1}}{2} - W\left(\frac{z_{k,j} + z_{k,j+1}}{2}\right)$$

where W is the windspeed at the midpoint's altitude. The lift generated by the tethers is not considered in this formulation. The contribution of the tether drag forces to the generalized forces acting on the generalized coordinates $X_{k,j}$ is given by

$$F_T^{k,j} = \frac{F_S^{k,j} + F_S^{k,j+1}}{2}.$$

E. Generalized Forces

The vector of generalized forces $F = \left[F_{1,1}^T, \ldots, F_{N,N_N}^T\right]^T$, where $F_{k,j} \in \mathbb{R}^3$ is the vector of generalized forces acting on the vector of generalized coordinates $X_{k,j}$, is resulting from the sum of the various contributions coming from tether drags

and airfoil aerodynamic forces. Though this summation can be performed very intuitively, it can be formulated as the following systematic construction. For any $k \in \{1, \ldots, N\}$, $j \in \{1, \ldots, N_k\}$, $F_{k,j}$ is given by

$$F_{k,j} = \begin{cases} F_T^{1,1}, & \text{if} \quad j = 1, \ k = 1 \\ F_T^{k,j}, & \text{if} \quad j \in 2, \ldots, N_k - 1 \\ F_T^{k,j} + \sum F_T^{k_c,1}, & \text{if } \mathcal{F}(k_c) = k \text{ and } j = N_k \\ F_T^{k,j} + F_{\mathrm{A}}^k, & \text{if} \quad k \in A \text{ and } j = N_k. \end{cases}$$

F. System Model

In the following, the generalized coordinate vector $X = [X_{1,1}^T, \ldots, X_{N,N_N}^T]^T$ of the system is used. The system is considered a set of independent tethers and airfoils, with associated Lagrange functions. The tethers introduce a set of constraints in the system configuration, given by

$$G_{k,j} = \frac{1}{2}\left((X_{k,j+1} - X_{k,j})^T (X_{k,j+1} - X_{k,j}) - l_{k,j}^2\right) = 0 \tag{2}$$

for $k = 1, \ldots, N$, $j = 1, \ldots, N_k$. The system Lagrange function reads as follows:

$$\mathcal{L} = \mathcal{T} - \mathcal{V} - \lambda^T G, \quad \mathcal{T} = \mathcal{T}_A + \mathcal{T}_T, \quad \mathcal{V} = \mathcal{V}_A + \mathcal{V}_T$$

where $\lambda \in \mathbb{R}^K$ is the vector of Lagrange multipliers associated to the constraints G. Using the Lagrange equation [9] $d/dt\ \partial\mathcal{L}/\partial\dot{X} - \partial\mathcal{L}/\partial X = F$, it can be verified that the system dynamics are given by the following index-3 DAEs as follows:

$$\mathcal{T}_{\dot{X}\dot{X}}\ddot{X} + G_X^T\lambda + \mathcal{V}_X = F, \qquad G = 0 \tag{3}$$

where λ is the DAE algebraic state, $G_X = \partial G/\partial X$, $\mathcal{T}_{\dot{X}\dot{X}} = \partial^2\mathcal{T}/\partial\dot{X}^2$ and $\mathcal{V}_X = \partial\mathcal{V}/\partial X$.

For any $t_0 \in \mathbb{R}$, (3) can be reformulated as an index-1 DAE by performing index reduction, which yields $\ddot{G}(t) = 0$, $\dot{G}(t_0) = 0$, and $G(t_0) = 0$. The resulting equations are read (together with the consistency conditions) as follows:

$$\begin{bmatrix} \mathcal{T}_{\dot{X}\dot{X}} & G_X^T \\ G_X & 0 \end{bmatrix} \begin{bmatrix} \ddot{X} \\ \lambda \end{bmatrix} = \begin{bmatrix} F - \mathcal{V}_X \\ -\frac{\partial}{\partial X}\left(G_X\dot{X}\right)\dot{X} \end{bmatrix} \tag{4}$$

$$G(t_0) = 0, \qquad \dot{G}(t_0) = \left(G_X\dot{X}\right)_{t=t_0} = 0. \tag{5}$$

It can be verified that the tension in tether k is readily given by

$$\Gamma_k = \lambda_k l_k.$$

For long integration times, a correction of the numerical drift of G may be required.

Equation (4) can be treated as an ODE by inverting the DAE mass matrix so as to compute $\ddot{X}$ and λ explicitly. Although this approach sounds appealing, and can be efficient for model simulations if the mass matrix is inverted numerically, the symbolic expressions for the resulting ODE are highly complex and the sparsity in the model expressions is usually lost. Therefore, computing the model sensitivities given in its ODE formulation is very expensive. In the framework of optimization, the system model is therefore best treated in the implicit form (4), using implicit integration methods.

1) Dual-Airfoil Model: The system architecture reads (Fig. 3) as follows:

$$N = 3, \quad \mathcal{A} = \{2, 3\}, \quad \mathcal{F}(1) = 0, \quad \mathcal{F}(2) = 1, \quad \mathcal{F}(3) = 1$$

the coordinate vector is $X \in \mathbb{R}^{3(N_1+N_2+N_3)}$ and the constraints are defined by

$$G = \frac{1}{2}\begin{bmatrix} \left((X_{1,2} - X_{1,1})^T (X_{1,2} - X_{1,1}) - l_{1,1}^2\right) \\ \vdots \\ \left((X_{1,N_1} - X_{1,N_1-1})^T (X_{1,N_1} - X_{1,N_1-1}) - l_{1,N_1-1}^2\right) \\ \left((X_{2,2} - X_{2,1})^T (X_{2,2} - X_{2,1}) - l_{2,1}^2\right) \\ \vdots \\ \left((X_{2,N_2} - X_{2,N_2-1})^T (X_{2,N_2} - X_{2,N_2-1}) - l_{2,N_2-1}^2\right) \\ \left((X_{3,2} - X_{3,1})^T (X_{3,2} - X_{3,1}) - l_{3,1}^2\right) \\ \vdots \\ \left((X_{3,N_3} - X_{3,N_3-1})^T (X_{3,N_3} - X_{3,N_3-1}) - l_{3,N_3-1}^2\right) \end{bmatrix}$$

where $X_{1,1} = X_0 = [0, \ 0, \ 0]^T$, the joint position is $X_{1,N_1} = X_{2,1} = X_{3,1} = X_1$, the first-airfoil position is $X_{2,N_2} = X_2$, and the second-airfoil position is $X_{3,N_3} = X_3$. The two airfoils and the two secondary tethers are considered identical. Thus, the discretization is also identical and $N_2 = N_3$.

2) Single-Airfoil Model: The system architecture reads (Fig. 2) as follows:

$$N = 1, \quad \mathcal{A} = \{1\}, \quad \mathcal{F}(1) = 0$$

the coordinate vector is $X \in \mathbb{R}^{3N_1}$ and the constraints are defined by

$$G = \frac{1}{2}\begin{bmatrix} \left((X_{1,2} - X_{1,1})^T (X_{1,2} - X_{1,1}) - l_{1,1}^2\right) \\ \vdots \\ \left((X_{1,N_1} - X_{1,N_1-1})^T (X_{1,N_1} - X_{1,N_1-1}) - l_{1,N_1-1}^2\right) \end{bmatrix}$$

where $X_{1,1} = X_0 = [0, \ 0, \ 0]^T$ and $X_{1,N_1} = X_1$.

G. Model Assumptions and Discussion

The proposed model is based on the following assumptions.

1) The tethers are modeled with a lumped-mass FEM.
2) The lift forces are orthogonal to the airfoil transversal axis.
3) The airfoils have a perfect yaw control, resulting in no side-slip.
4) The time-derivatives of the lift coefficient and roll angle are controlled and actuation is instantaneous.
5) The time-derivative of the onboard turbine drag coefficient is controlled and actuation is instantaneous.

The proposed model construction can straightforwardly accommodate different tether and airfoil models, e.g., a six-DOF-airfoil description and more elaborate aerodynamic models. Yet in this brief, a simple model is preferred, so as to reduce the complexity of the presentation. Further research will seek improving the tether models by including the tether aerodynamic lift and elasticity.

In this brief, no assumption is made on the interaction between the airfoils and the airmass. For conventional wind turbines, Betz first developed a simplified model [3], [19].

Although such a formulation can be adapted for AWE systems and included in the problem formulation, experimental data is needed to assess the validity of such a simplified model. This validation process is the subject of ongoing research at KU Leuven.

III. Optimization Problem

The airfoil trajectories as well as the tether lengths and sections are manipulated so as to maximize the system average power generation over an orbit of free duration T_p. The periodicity of the system is guaranteed by satisfying the boundary conditions as follows:

$$X(0) - X(T_p) = 0. \tag{6}$$

However, it can be observed that (6) together with (5) form a redundant set of equality constraints, violating the linear independence constraint qualification. The directions violating the consistency conditions must then be removed from the set of periodicity conditions [6]. Defining a matrix Z that forms a basis of the null-space of

$$J = \left[\begin{array}{c} \frac{\partial G}{\partial X} \\ \frac{\partial G}{\partial X} \end{array} \right]_{t=0}$$

i.e., $JZ = 0$, the set of consistency conditions (5) together with

$$Z^T (X(0) - X(T_p)) = 0 \tag{7}$$

have no redundancy. The basis Z is nonunique, and can be chosen so as to limit its computational complexity. As an alternative, it can also be introduced as a set of parameters in the optimization algorithm, and computed numerically.

To ensure that the tethers are always under tension but that their resistance is never exceeded, the constraints are as follows:

$$\frac{\gamma}{f_s} \frac{\pi}{4} d_k^2 \geq \Gamma_k(t) = \lambda_k l_k \geq 0 \quad \forall t,\ k = 1, \ldots, N \tag{8}$$

are imposed, where γ is the tether yield strength and f_s is the safety factor. In addition, the following bounds are proposed as follows:

$$\begin{aligned} 0 \leq C_{\mathrm{L}}^i \leq 1, \qquad & -5\ \mathrm{s}^{-1} \leq \dot{C}_{\mathrm{L}}^i \leq 5\ \mathrm{s}^{-1} \\ -80^\circ \leq \psi_L^i \leq 80^\circ, \qquad & -5\ \mathrm{s}^{-1} \leq \dot{\psi}_L^i \leq 5\ \mathrm{s}^{-1} \\ -1000\ \mathrm{kg/(ms)} \leq \dot{\kappa}_i \leq 1000\ \mathrm{kg/(ms)} \qquad & \forall t,\ i \in \mathcal{A}. \end{aligned} \tag{9}$$

The periodic power optimization problem reads as follows:

$$\begin{aligned} \bar{P} = \max_{U, X, \theta, T_p} \quad & \frac{1}{T_p} \int_0^{T_p} \sum_{i \in \mathcal{A}} P_i dt \\ \text{s.t.} \quad & (4) - (5), (7) - (9) \end{aligned} \tag{10}$$

where $U_i = \{\dot{C}_{\mathrm{L}}^i,\ \dot{\psi}_L^i,\ \kappa_i\}$, $i \in \mathcal{A}$, $\theta_k = \{l_k,\ d_k\}$, $k = 1, \ldots, N$. T_p is an optimization variable, thus the duration of the orbit will be adapted by the optimizer so as to maximize the average power. To be able to treat this problem, a time transformation can be introduced, as proposed in [10, p. 27].

TABLE I
Fixed Model Parameters

Parameter	Symbol	Value	Unit
Air density	ρ	1.23	$\mathrm{kg \cdot m^3}$
Tethers density	ρ_c	1450	$\mathrm{kg \cdot m^3}$
Airfoil parasitic drag coefficient	C_D^0	0.02	–
Airfoil induced drag coefficient	C_D^I	0.02	–
Airfoil aspect ratio	A_R	10	–
Wind velocity at altitude z_0	W_0	10	m/s
Altitude of wind velocity W_0	z_0	100	m
Roughness factor	z_r	0.1	m
Sea level standard temperature	T_0	288.15	K
Temperature lapse rate	T_L	0.0065	K/m
Sea level pressure	P_0	101325	Pa
Molar air density	M_a	0.0289644	kg/mol
Universal gas constant	R	8.31447	J/(molK)
Tether drag coefficient	C_T	1	–
Tether yield strength	γ	$3.9 \cdot 10^9$	Pa
Safety factor	f_s	5	–

A. Solution Approach

The optimal control problem (10) is large-scale and highly nonconvex and therefore requires a good initial guess to be tackled by derivative-based optimization. However, no such guess is readily available. To address this issue, a complex procedure is needed to compute an initial guess for problem (10). For the sake of brevity, the details of this procedure will be omitted.

For the dual-airfoil system, solving (10) on a full orbit yields quasi-identical trajectories for the two airfoils, hence (10) is solved on a half orbit instead, using the periodicity conditions $X_2(0) = X_3(1/2T_p)$, $X_3(0) = X_2(1/2T_p)$ so as to match the terminal state of one airfoil with the initial state of the other. For both the single and dual-airfoil problems, the control input profiles are discretized using a piecewise-constant parameterization having 20 intervals/full orbit. One collocation element is used per control interval.

B. Methods & Software

Because dynamics (4) are unstable, a simultaneous optimal control technique is required to optimize the system model. In this brief, the discretization of the model dynamics (4) is based on a direct collocation approach [4], where the model simulation, constraints, and optimization are handled simultaneously in a large-scale sparse nonlinear program (NLP). Collocation approaches provide a straightforward way to deal with implicit index-1 DAE systems [4].

The problem transcription is performed using the open-source optimization framework CasADi [1]. The resulting NLP is solved using the interior-point solver IPOPT 3.10.1 [23] using WSMP as a linear solver.

IV. Parametric Study

The parametric studies aim at assessing the relationship between the total airfoil surface and the average generated power, i.e., $\bar{P}\ (S_{\mathrm{tot}})$ where $S_{\mathrm{tot}} = \sum_{n \in \mathcal{A}} S$. This brief focused

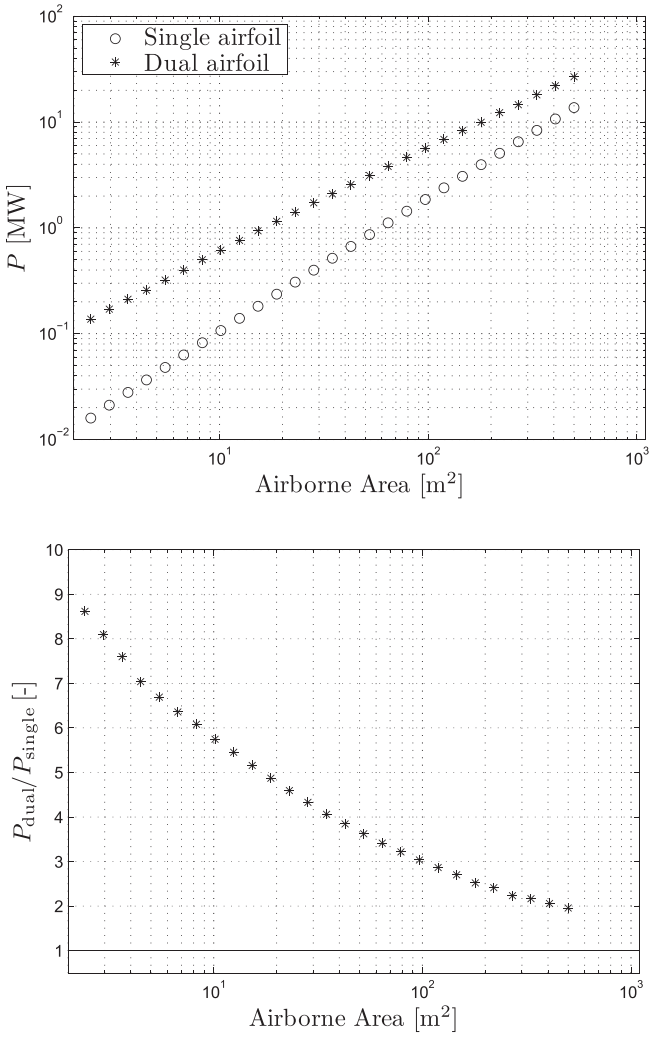

Fig. 4. Dual versus one large single airfoil: average power output for different wing surface S, keeping the wing loading constant. The comparison assumes that both systems have the same overall airfoil surface, i.e., $S_{\text{dual}} = 1/2 S_{\text{single}}$, hence assessing the advantage of having a dual-airfoil system with two smaller airfoils versus having a single large airfoil.

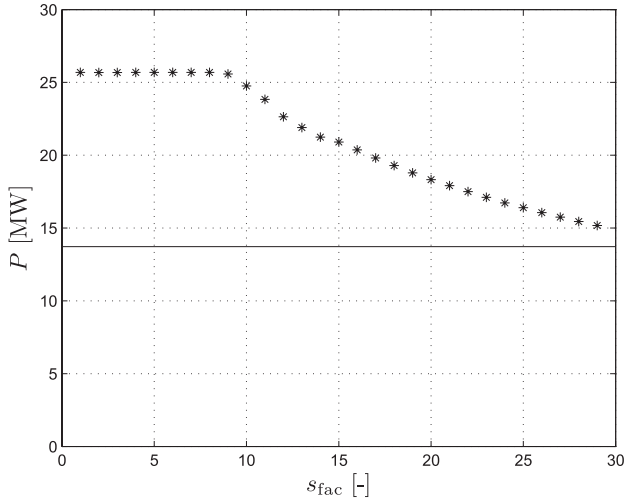

Fig. 5. Study of the impact of the safety constraint on the extracted power P for the largest dual-airfoil system. The parameter s_{fac} is the distance between the airfoils, measured in wingspans. For comparison, the energy extracted by the single airfoil is displayed as a continuous line.

on assessing whether, for a given total airfoil surface, a single- or a dual-airfoil system should be preferred.

This brief is based on airfoils having a maximum gliding ratio $L/D = 25$. The tethers are assumed to be made of Dyneema, which has a very high stiffness and yield strength for a low density. The fixed model parameters are summarized in Table I.

For the single airfoil, the tether is discretized using five segments. For the dual airfoils, the main tether is discretized using 20 segments, whereas five segments are used for both secondary tethers. This results in 41 states for the single airfoil and 207 states for the dual airfoils. More refined tether discretizations are tested and the obtained results do not show any relevant difference.

Problem (10) being nonconvex, there is no *a priori* guarantee that the computed solution is a global optimum. Nevertheless, using insights on the physics of the system, it is possible to assess the solution and compare it with the results of simplified studies, such as the ones proposed in [17]. Initializing problem (10) at different initial guesses, it is observed that the NLP solver consistently converges to the same solution, hence suggesting that it is the optimum of a reasonably large set of possible trajectories.

Using the method proposed in Section III-A a solution to (10) for the single-airfoil system using parameter values $S = 500$ m^2 and $M_A/S = 20$ kg/m^2, and a solution for the dual-airfoil system using parameter values $S = 250$ m^2 and $M_A/S = 20$ kg/m^2 are computed.

Starting from these solutions, a homotopy with respect to the total airfoil area S_{tot} is applied to (10). Keeping the wing loading $M_A/S = 20$ kg/m^2 constant (i.e., the airfoil mass scales linearly with the total airfoil area), S_{tot} is gradually reduced and (10) repeatedly solved, using the solution from the previous step as an initial guess for the subsequent steps. The average generated power for both the single- and dual-airfoil systems is shown the top graph of Fig. 4. The ratio between the average generated power for the dual-airfoil system and the single-airfoil system the bottom graph of Fig. 4. The graphs in Fig. 4 show the mechanical power dissipated by the onboard turbines. The actual electrical power depends on the generators and converters efficiency, whose value is arguably similar for the two systems. For the chosen parameters, the dual-airfoil system is always more advantageous than the single one. As the total airfoil surface increases, however, the ratio between the power extracted by the dual and single airfoil decreases significantly.

It should be observed that the required total airfoil surface for a desired amount of average generated power is also indirectly assessed through the proposed parametric study. Indeed, from Fig. 4, an average power generation of 10 MW the dual-airfoil system requires a total airfoil surface of approximately half the one of the single-airfoil system, but the dual-airfoil system requires gradually less airfoil surface as the desired average generated power decreases.

For safety reasons, it is desirable that the dual-airfoil trajectories keep the airfoils far from each other, thus avoiding the risk of collisions. A second reason for having the airfoils flying

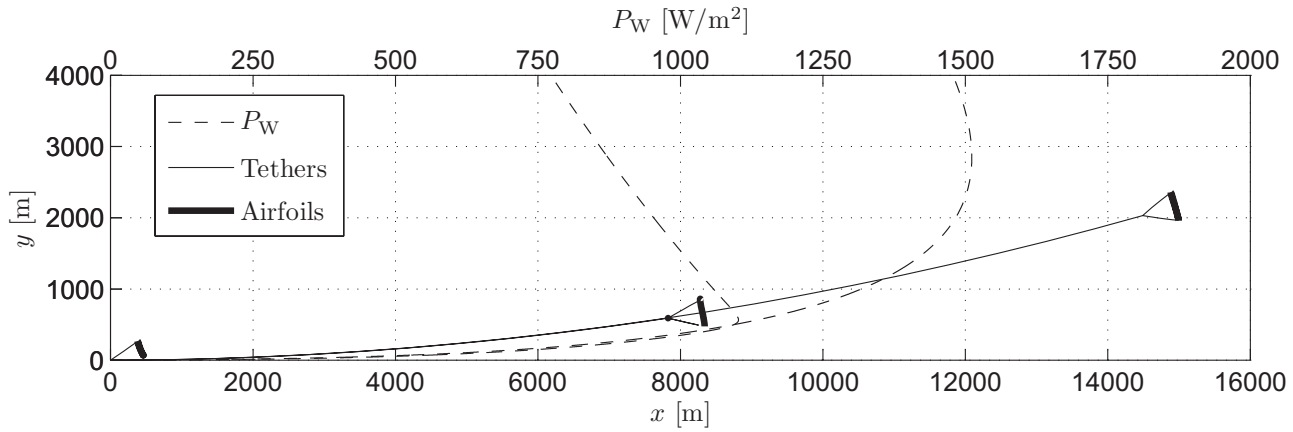

Fig. 6. Trajectory comparison between the single and dual airfoils for a total wing surface $S_{\text{tot}} = 500$ m^2. Trajectories (thick lines) and available wind power $P_w = \rho W_\infty^3/2$ (dashed line). For the dual airfoils, two wind profiles are considered: (a) logarithmic profile (1) and (b) logarithmic profile saturated above $z = 500$ m.

large orbits, is to reduce the interaction with the airmass. In this brief, no hypothesis is made on this complex interaction, which is assumed to be small and is thus neglected. This assumption might not hold if the airfoils fly too close to each other, as the interaction will be higher. Thus, a study is done, to check how the extracted power is affected by imposing a safety constraint on the distance between the airfoils. This safety constraint is expressed as follows:

$$(X_2 - X_3)^T (X_2 - X_3) \geq (s_{\text{fac}} w_{\text{s}})^2 \tag{11}$$

where the wingspan is given by $w_s = \sqrt{SA_R}$, with A_R the aspect ratio. For the simulations, the value $A_R = 10$ is chosen. The results are shown in Fig. 5 for the largest dual-airfoil system, i.e., $S_{\text{tot}} = 500$ m^2. Allowing the airfoils to fly closer than 9 w_s does not lead to an increase in the extracted power. For larger orbits, the extracted power diminishes but the loss is not dramatic and, even for very large orbits, the dual airfoils still extract more power than the single airfoil.

The trajectory for the biggest systems considered, i.e., $S_{\text{tot}} = 500$ m^2, is shown in Fig. 6. The dual airfoils operate at much higher altitude, approaching the peak of the available wind power formula (2850 m), also shown in Fig. 6. The proposed wind shear model (1) is valid only in the atmospheric boundary layer, which is typically lower than 2000 m. In this brief, the boundary layer is supposed to have an infinite thickness. The resulting optimal trajectories for the dual-kite systems reach over 2000 m, which strongly suggest that the optimal altitude is always at the top of the boundary layer, regardless of its thickness. Arguably, in boundary layers that are not developed to the top altitude of 2000 m, the dual-airfoil system would loose some of its efficiency, and its advantage over the single-airfoil system would be reduced. In regard of these results, in practice, the optimization of a dual-airfoil AWE system should consider the average altitude of the boundary layer in the region of interest. As a term of comparison, a second scenario is considered, where the wind profile saturates for $z > 500$ m. The resulting trajectory and related available wind power are also shown in Fig. 6. In this second case, the trajectory is still in proximity of the peak of available wind power, which occurs at much lower altitude. For a total wing surface $S_{\text{tot}} = 500\,\text{m}^2$, also in a saturated wind profile, the power extracted by the dual airfoils exceeds the one extracted by the single airfoil by the ratio $P_{\text{dual}} = 1.54\ P_{\text{single}}$.

The tether length obtained for the dual-kite system is arguably extremely large. It is observed, however, that the sensitivity of the power generation to the tether length is rather small, i.e., constraining the tether to smaller length does not result in a large power loss. Arguably, economical factors such as the material cost and the electrical resistance of a very long tether would yield a system with a shorter tether. In this brief, however, only the physics of the system are considered.

To check the precision of the collocation discretization, an optimization for the biggest system runs with a refined collocation scheme having four times more collocation elements, resulting in an NLP with 47 350 variables. No relevant difference is noticed in the resulting trajectory, suggesting that the chosen collocation scheme is accurate enough.

The proposed scenario assumes the airfoils do not modify the wind field. The development of an accurate model needs extensive studies. Future research will aim at investigating the impact of the presence of the airfoils on the wind field. Early results relying on simplified interaction models suggest that the dual airfoils would still extract more power than the single airfoil. Yet, a higher performance loss is observed for the dual-airfoil system.

Observe that the computed trajectories are only valid for the nominal case and in a real application wind perturbations and unmodeled dynamics will affect the performance of the system: this problem can be tackled within a robust optimization framework. The resulting NLP will, though, be considerably more complex than the proposed one. In the context of a real application, performance is also affected by the choice of the controller. Both investigations are out of the scope of this brief and are the subject of ongoing research.

V. Conclusion

This brief proposed a generic multiple-airfoil modeling procedure of minimal computational complexity, aimed for the optimization of power generation. This procedure can straightforwardly accommodate for six-DOF airfoil models.

The proposed procedure was applied to develop a large-scale model for the comparison of single versus dual-airfoil systems so as to investigate which system was best suited, given the required average power output.

The results showed that dual systems extracted more power for all scales on the given scenario. Scaling up from small to large scales, the ratio of the power extracted by the dual airfoils versus the one extracted by the single airfoil decreased.

Tether elasticity was neglected and the airfoil model was simplified for the sake of clarity of the presentation. Future research will focus on building a model database for both airfoils and tethers to be interfaced to the modeling procedure and optimization routines proposed.

For more accurate study, the interaction between the airfoils and the airmass should be included in the model. A computational fluid dynamics simulation is the object of ongoing research.

ACKNOWLEDGMENT

The authors would like to thank A. Kozma for his technical support and Reinhart Paelinck for the illustration in Fig. 1.

REFERENCES

[1] J. Andersson, J. Åkesson, M. Diehl, S. Forth, P. Hovland, E. Phipps, J. Utke, and A. Walther, "CasADi–A symbolic package for automatic differentiation and optimal control," in *Proc. 6th Int. Conf. Autom. Differ.*, 2012, pp. 297–307.

[2] D. G. Andrews. *An Introduction to Atmosphere Physics*. Cambridge, U.K.: Cambridge Univ. Press, 2010.

[3] F. D. Bianchi, B. H. de Mantz, and J. Ricardo, *Wind Turbine Control Systems*. New York, NY, USA: Springer-Verlag, 2007.

[4] L. T. Biegler, "Nonlinear programming," in *MOS-SIAM Series on Optimization*. Philadelphia, PA, USA: SIAM, 2010.

[5] E. A. Bossanyi, "Further load reductions with individual pitch control," *Wind Energy*, vol. 8, no. 4, pp. 481–485, Oct.–Dec. 2005.

[6] S. Boyd and L. Vandenberghe, *Convex Optimization*. Cambridge, U.K.: Cambridge Univ. Press, 2004.

[7] M. Canale, L. Fagiano, and M. Milanese, "High altitude wind energy generation using controlled power kites," *IEEE Trans. Control Syst. Technol.*, vol. 18, no. 2, pp. 168–180, Mar. 2010.

[8] M. V. Cook, *Flight Dynamics Principles*. New York, NY, USA: Elsevier Science, 2007.

[9] J. García de Jalón, and E. Bayo, *Kinematic and Dynamic Simulation of Multibody Systems: The Real-Time Challenge*. New York, NY, USA: Springer-Verlag, 1994.

[10] M. Diehl, "Real-time optimization for large scale nonlinear processes," Ph.D. dissertation, Dept. Appl. Math., Univ. Heidelberg, Heidelberg, Germany, 2001.

[11] M. Diehl and B. Houska, "Windenergienutzung mit schnell fliegenden flugdrachen: Eine herausforderung für die otimierung und regelung-wind power via fast flying kites: A challenge for optimization and control," *Automatisierungstechnik*, vol. 57, no. 10, pp. 525–533, 2009.

[12] L. Fagiano, M. Milanese, and D. Piga, "High-altitude wind power generation," *IEEE Trans. Energy Convers.*, vol. 25, no. 1, pp. 168–180, Mar. 2010.

[13] L. Fagiano, M. Milanese, and D. Piga, "Optimization of airborne wind energy generators," *Int. J. Robust Nonlinear Control*, vol. 22, no. 18, pp. 2055–2083, Dec. 2011.

[14] B. Houska and M. Diehl, "Optimal control of towing kites," in *Proc. 45th IEEE Conf. Decision Control*, Dec. 2006, pp. 2693–2697.

[15] B. Houska and M. Diehl, "Optimal control for power generating kites," in *Proc. 9th Eur. Control Conf.*, 2007, pp. 3560–3567.

[16] J. H. Laks, L. Y. Pao, and A. D. Wright, "Control of wind turbines: Past, present, and future," in *Proc. Amer. Control Conf.*, 2009, pp. 2096–2103.

[17] M. L. Loyd, "Crosswind kite power," *J. Energy*, vol. 4, no. 3, pp. 106–111, Jul. 1980.

[18] *Makani Power Homepage*. (2012) [Online]. Available: http://www.makanipower.com

[19] J. F. McGowan, J. G. McGowan, and A. L. Rogers, *Wind Energy Explained: Theory, Design and Application*, 2nd ed. New York, NY, USA: Wiley, 2009.

[20] B. Pamadi, *Performance, Stability, Dynamics, and Control of Airplanes*, 2nd ed. Reston, VA, USA: AIAA, 2003.

[21] P. Payne and C. McCutchen, "Self-erecting windmill," U.S. Patent 3 987 987, Oct. 26, 1976.

[22] A. R. Podgaets and W. J. Ockels, "Flight control and stability of a multiple kites tethered system," in *Proc. Renew. Energy Conf.*, 2006, pp. 1–4.

[23] A. Wächter and L. T. Biegler, "On the implementation of a primal-dual interior point filter line search algorithm for large-scale nonlinear programming," *Math. Program.*, vol. 106, no. 1, pp. 25–57, 2006.

[24] P. Williams, B. Lansdorp, and W. Ockels, "Optimal crosswind towing and power generation with tethered kites," *J. Guid., Control, Dynamics*, vol. 31, no. 1, pp. 81–92, Jan.–Feb. 2008.

[25] P. Williams, B. Lansdorp, and W. J. Ockels, "Modeling of optimal power generation using multiple kites," in *Proc. AIAA Model. Simul. Technol. Conf. Exhibit*, Aug. 2008, pp. 1–4.